Molecular dynamics study of the thermal conductivity of amorphous nanoporous silica

Thomas Coquil, Jin Fang, Laurent Pilon *

University of California, Los Angeles Henry Samueli School of Engineering and Applied Science, Mechanical and Aerospace Engineering Department, 420 Westwood Plaza, Los Angeles, CA 90095, United States

A R T I C L E   I N F O

A B S T R A C T

This study reports, for the first time, non-equilibrium molecular dynamics (MD) simulations predicting the thermal conductivity of amorphous nanoporous silica. The heat flux was imposed using the Müller-Plathe method and interatomic interactions were modeled using the widely used van Beest, Kramer and van Santen potential. Monodisperse spherical pores organized in a simple cubic lattice were introduced in an amorphous silica matrix by removing atoms within selected regions. The simulation cell length ranged from 17 to 189 Å, the pore diameter from 12 to 25 Å, and the porosity varied between 10% and 35%. Results establish that the thermal conductivity of nanoporous silica at room temperature was independent of pore size and depended only on porosity. This qualitatively confirms recent experimental measurements for cubic and hexagonal mesoporous silica films with pore diameter and porosity ranging from 3 to 18 nm and 20% to 48%, respectively. Moreover, predictions of MD simulations agreed well with predictions from the coherent potential model. By contrast, finite element analysis simulating the same nanoporous structures, but based on continuum theory of heat conduction, agreed with the well-known Maxwell Garnett model.

1. Introduction

Nanoporous silica consists of nanoscale pores (0.1 nm–1 μm) embedded in an amorphous silica matrix. They are being considered as ultra-low-k dielectric interlayer materials for their low dielectric constant [1]. However, by introducing nanoscale pores into the dielectric material, not only the effective dielectric constant but also the thermal conductivity substantially decreases. Then, nanoporous silica acts as a thermal insulator and may constitute a barrier to efficient heat removal. Nanoporous silica thin films have also been used for thermal insulation of infrared detectors and various MEMS devices [2]. In these applications, knowledge of the thermal conductivity of nanoporous silica thin films is essential for the design and thermal management of devices.

Predicting the thermal conductivity of amorphous nanoporous materials is very challenging because of their disordered atomic structures and the presence of nanopores presenting large matrix/pore interfacial area and resistance to energy transport through the nanostructure. Effective medium approximations (EMAs) predicting the thermal conductivity of such complex materials can vary widely and were shown to be inaccurate [3]. On the other hand, classical molecular dynamics (MD) simulations are based on a limited number of assumptions aside from the interaction potential and represent an alternative to both experiments and EMAs. They can also provide insight into the physical phenomena controlling energy transport in nanostructured materials.

In this manuscript, the thermal conductivity of nanoporous amorphous silica thin films is predicted using non-equilibrium MD simulations for various cell length, spherical pore diameter, and porosity. Results are compared with (i) recent experimental measurements for highly ordered mesoporous silica thin films [3] and (ii) predictions based on continuum theory of heat conduction in porous media.

2. Background

Three different methods have been used to determine the thermal conductivity of materials using MD simulations, namely (i) the equilibrium method using the Green–Kubo relations [4–6], (ii) the direct non-equilibrium method [4,7], or (iii) the Müller-Plathe method [8]. The first method consists of retrieving the thermal conductivity at equilibrium through linear response theory using relations derived by Green [5] and Kubo et al. [6]. Indeed, perturbations are induced by the fluctuations of the system temperature at equilibrium. The response of the system to these perturbations is determined by its thermal conductivity. In a so-called NVE ensemble defined by constant number of atoms, volume, and energy, the

* Corresponding author. Tel.: +1 310 206 5598; fax: +1 310 206 2302.
  E-mail address: pilon@seas.ucla.edu (L. Pilon).

Nomenclature

A_{ij}	parameter in the BKS potential [eV]
B_{ij}	parameter in the BKS potential [Å^{-1}]
C_{ij}	parameter in the BKS potential [eV · Å^6]
d_p	pore diameter [m]
f_v	porosity
k_B	Boltzmann constant [$k_B = 1.38 \times 10^{-23}$ m^{2}kg/s^{2}K]
k	thermal conductivity [W/m · K]
k_c	the thermal conductivity of the silica matrix [W/m · K]
k_d	the thermal conductivity of air in the pore [W/m · K]
$k_{d,0}$	thermal conductivity of bulk air (Kn = 0.0)
Kn	Knudsen number [Eq. (5)]
ℓ	gas molecule mean free path [m]
L_z	simulation cell length [m]
m_i	mass of atom i [kg]
N	number of slices
n	number of atoms
p	pressure inside the pore [N/m^2]
q	atomic charge [e]
q_z''	heat flux [W/m^2]
r_{ij}	interatomic distance between atoms i and j [Å]
S	simulation cell cross-section [m^2]

T	temperature [K]
v_i	velocity of atom i [m/s]
$V(r_{ij})$	interatomic potential [eV]
z	distance along the direction of heat propagation [m]

Symbols

β	coefficient in Eq. (5)
ϵ_{ij}	depth of the L–J potential well between atoms i and j [eV]
σ	diameter of the hard-shell particles representing gas molecules [m]
σ_{ij}	characteristic distance in the L–J potential between atoms i and j [Å]

Subscripts

i, j	refers to individual atom i or j
k	refers to the kth slice
O	refers to oxygen atom
Si	refers to silicon atom

thermal conductivity can thus be evaluated through the time integration of the auto-correlation function of the energy current [9]. Indeed, the energy current vector indicates the direction and amount of energy transfer in the system at an instant in time. The thermal conductivity of the system determines how long this energy current remains correlated with itself. In a material with a large thermal conductivity, the correlation will be long lasting because fluctuations from equilibrium dissipate slowly. On the other hand, the correlation will be short lived in materials with low thermal conductivity. This method has already been implemented to estimate the thermal conductivity of fluid and solid systems such as argon [10], diamond [11], β-silicon carbide [12], silicon [7,13] or silica [14], for example.

The two other methods, on the contrary, are performed under non-equilibrium conditions. The direct non-equilibrium MD simulations, consist of imposing a temperature gradient across the system by analogy with experimental measurements. Alternatively, the Müller-Plathe method consists of imposing a heat flux to the system and estimating the resulting temperature gradient. These methods have been implemented to predict the thermal conductivity of (i) bulk dense silicon [7] using the Stillinger and Weber potential [15] as well as that of (ii) dense silica [16–18] and amorphous silica nanoparticles or nanowires [9] using the the so-called BKS potential proposed by van Beest, Kramer and van Santen [19].

The literature mostly reports MD simulations performed on bulk dense materials [4,7,11,12,16,14,17,18,20–22]. Numerous studies have discussed the effects of the finite size of the simulation cell on thermal conductivity predictions [7,11,14,16,17,20–22]. These effects are mostly due to the limited mean free path of the phonons that can be simulated [22]. Finite size effects are expected to be larger in crystalline than in amorphous systems because phonons have shorter mean free paths in amorphous materials. On the other hand, very few studies [9,11,23–26] have focused on modeling the thermal conductivity of nanostructured materials where finite-size effects may also be caused by the actual geometry of the structure simulated. Che et al. [11] simulated the thermal conductivity of carbon nanotubes (CNTs) made of up to 6,400 atoms at 300 K using the Green–Kubo method. Lukes and

Zhong [27] reported the thermal conductivity, phonon density of states, and phonon relaxation times for single-wall CNTs of various length from 100 K to 500 K. Recently, Thomas et al. [25] used the direct non-equilibrium method to predict the thermal conductivity at 300 K of empty and water-filled CNTs consisting of nearly 200,000 atoms. The authors explored the transition to fully diffusive phonon transport with increasing CNT length. In a second study [26], they presented a method for predicting phonon dispersion relations and lifetimes from MD simulations and applied it to CNTs. Thermal conductivities calculated from the phonon properties were in excellent agreement with those obtained from direct MD simulations [25]. Mahajan et al. [9] modeled the thermal conductivity of both amorphous silica nanoparticles and nanowires made of 600 atoms at 300 K using the Müller-Plathe method. Lukes and Tien [23] reported the thermal conductivity of nanoporous thin films of Argon using MD simulations with a simple Lennard–Jones (LJ) potential. They investigated the effects of average temperature, pore location, shape, size, and orientation on the film thermal conductivity. The results showed that larger porosities and higher temperatures yielded lower thermal conductivity. However, pore shape and arrangement did not significantly influence thermal conduction while effects of orientation were noticeable only for the most anisotropic cases. Note that this study was limited to systems with less than 1,000 atoms and simulated only one or two pores smaller than 2 nm in diameter. Finally, Lee et al. [24] investigated the thermal conductivity of nanoporous silicon with porosity ranging from 7% to 38% and cylindrical pores with diameter ranging from 0.63 to 2.26 nm. The predicted thermal conductivity was two orders of magnitude smaller than that of dense silicon. Note that in this latter study, only one pore was considered.

He et al. [28] performed both equilibrium and non-equilibrium MD simulations as well as lattice dynamic simulations of amorphous silicon at 300 K. They showed that most heat carriers were non-propagating or quasi-stationary modes. The small fraction ($\sim$3%) of propagating phonon modes had mean free path of the order of 0.1–1 μm and contributed to about 50% of the total a-Si thermal conductivity. However, the presence of cylindrical nanoholes significantly reduced their mean free path causing a major reduction in the thermal conductivity.

The present study uses non-equilibrium classical molecular dynamics simulations and the Müller-Plathe method [8] to predict the thermal conductivity of amorphous nanoporous silica at room temperature. It is unique in that it investigates amorphous nanoporous silica systems with (i) more than 9,000 atoms, (ii) up to 11 pores, and (iii) a wide range of cross-sectional area, length, porosity, and pore diameter. The system length, porosity, and pore diameter investigated ranged from 17 to 189 Å, 10% to 35%, and 12 to 25 Å, respectively. First, the method was validated by comparing the predicted thermal conductivity of dense (non-porous) crystalline α-quartz and amorphous silica with data previously reported in the literature [9,16,17]. Then, the thermal conductivity of amorphous nanoporous silica systems was computed after introducing pores within the previously generated dense amorphous silica phases. Results were compared with (i) predictions from finite element simulations based on continuum theory for heat conduction, (ii) commonly used EMAs, and (iii) previously reported experimental data [3].

3. Analysis

3.1. Müller-Plathe method

The thermal conductivity, k, along the direction of heat propagation z is defined by Fourier's law as the ratio of the heat flux q''_z to the steady-state temperature gradient dT/dz,

$$k = -\frac{q''_z}{dT/dz} \tag{1}$$

Thermal conductivity can therefore be estimated in two different ways: (i) by imposing a temperature gradient and determining the resulting heat flux, or (ii) by imposing a heat flux and determining the resulting temperature gradient. Both methods can be implemented through non-equilibrium MD simulations. However, imposing a temperature gradient was not considered here due to the slow convergence of the heat flux value [8,29]. Instead, the previously mentioned Müller-Plathe method [8,9] was implemented. In this approach, the slowly converging quantity (i.e., the heat flux) was imposed through velocity rescaling. On the other hand, the temperature and its gradient were calculated by averaging the atomic kinetic energy over time and over a large number of atoms. To do so, the simulation cell was divided into an even number, $2N$, of plane-parallel slices along the direction of the heat flux as shown in Fig. 1. The temperature of each slice at every time step was determined from the classical statistical mechanics equipartition theorem as [9],

$$T_k = \frac{1}{3n_k k_B} \sum_{i=1}^{n_k} m_i v_i^2 \tag{2}$$

where n_k is the number of atoms in the kth slice and m_i and v_i are the mass and velocity of the ith individual atom. The temperature of each slice was then averaged over multiple time steps. Note that, Eq. (2) is valid if (i) the temperature gradient is not imposed, (ii) the total momentum of the system vanishes, and (iii) the heat capacity is independent of temperature [13].

The heat flux was imposed by exchanging velocities between atoms of the $(N+1)$th slice in the middle of the cell and atoms of the 1st slice at one end of the cell. The velocity of the atom with the largest kinetic energy (i.e., the hottest) of the 1st slice was exchanged with the velocity of the atom with the lowest kinetic energy (i.e., the coolest) of the $(N+1)$th slice. Note that those atoms had to be of identical mass so that the total linear momentum, kinetic energy, and total energy of the system were conserved [8]. However, the total angular momentum of the system may not be conserved [8]. Those velocity exchanges were performed every given number of simulation steps to impose a constant adjustable heat flux q''_z. After reaching steady state, a temperature profile $T(z)$, which decreased from the center to the ends of the simulation cell could be measured. Then, the thermal conductivity was retrieved using Eq. (1). In addition, in order to simulate bulk materials, periodic boundary conditions were imposed in all directions. This method had previously been implemented to predict the thermal conductivity of dense solid materials such as silicon [7] as well as quartz [17] and amorphous silica at temperatures 300 K [9] and between 100 and 700 K [16]. In the present study, this numerical procedure was implemented using the Large-scale Atomic/Molecular Massively Parallel Simulator (LAMMPS) [30]. Simulations were ran in parallel on eight to sixty-four 64-bit nodes with 1024 MB of RAM. The MD simulation method implemented in the present study was first validated by modeling the thermal conductivity of dense crystalline α-quartz. Results were systematically compared with those previously reported in the literature [9,16,17].

3.2. Validation: thermal conductivity of crystalline α-quartz

MD simulations of crystalline α-quartz were performed at 500 and 800 K following the procedure adopted by Yoon et al. [17]. The Müller-Plathe method was implemented. As in most studies modeling properties of silica based nanostructures [9,16–18], the BKS potential [19] was used. The BKS potential is a two body potential given by [19],

$$V(r_{ij}) = \frac{q_i q_j}{r_{ij}} + A_{ij} exp(-B_{ij} r_{ij}) - \frac{C_{ij}}{r_{ij}^6} \tag{3}$$

where r_{ij} is the distance separating two atoms i and j, q_i and q_j are the atomic charges of both atoms and A_{ij}, B_{ij} and C_{ij} are constants specified for each type of pair of atoms i and j. The values used for those parameters where the same as those initially defined in Ref. [19] and used by Yoon et al. [17] namely A_{SiSi} = 0.0 eV, A_{SiO} = 18,003.7572 eV, A_{OO} = 1,388.7730 eV, B_{SiSi} = 0.0 Å^{-1}, B_{SiO} = 4.87318 Å^{-1}, B_{OO} = 2.760 Å^{-1}, C_{SiSi} = 0.0 eV · Å^6, C_{SiO} = 133.5381 eV · Å^6, C_{OO} = 175.0 eV · Å^6, q_{Si} = 2.4 e, and q_O = − 1.2 e. The short-range cutoff, where interactions were computed in real space, was set to 8 Å [16]. The long-range Coulombic interactions beyond the short-range cutoff were calculated in reciprocal space using a particle–particle particle-mesh solver [31].

Simulations were performed using an α-quartz structure [32] at both 500 and 800 K with density equal to 2,647 kg/m^3 while the heat flux was imposed along the c-axis ([0001] direction). Fig. 2a shows the atomic structure of a typical α-quartz phase simulated, viewed down the c-axis. Periodic boundary conditions were
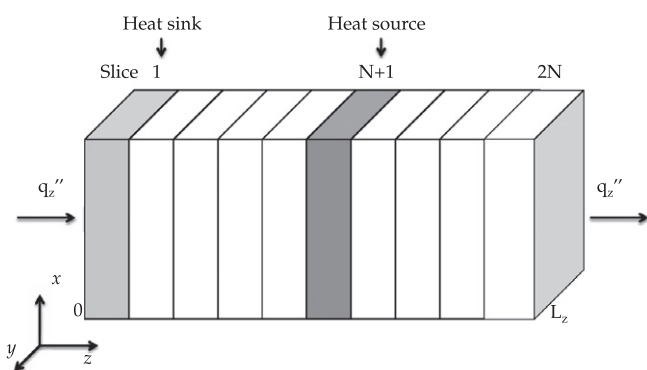

Fig. 1. Simulation cell divided into 2 N slices along the heat flux direction. Periodic boundary conditions were applied in all directions.
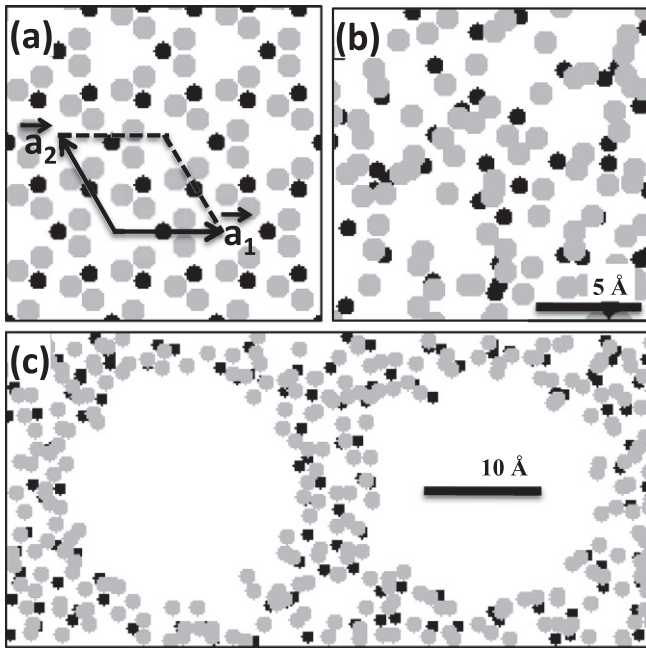
Fig. 2. Typical atomic structures of (a) α-quartz phase with the out-of-plane direction corresponding to the [0001] direction or c-axis, (b) amorphous silica phase, and (c) nanoporous amorphous silica phase with two spherical pores of 18 Å in diameter aligned along the z-direction of a 23.4 × 22.5 × 45.7 Å³ simulation cell. Note that these 2D representations correspond to the projection of a 8.5 Å thick slab in the out-of-plane direction.

Fig. 3. Predicted values of $1/k$ as a function of $1/L_z$ for crystalline α-quartz at 500 and 800 K along with results reported in the literature [16,17].

applied in all three directions and simulation cells had dimensions identical to those used by Yoon et al. [17]. The cross-section of the simulation cell was set to 4 × 4 repeat units of the α-quartz basal plane while its length, L_z, was set to 12, 16 and 20 times the α-quartz lattice parameter along the c-axis. The rate of velocity exchanges was chosen so that the corresponding heat flux was approximately 3.8×10^{11} eV/nm^2· s (i.e., 3×10^{10} W/m^2) by analogy with Yoon et al. [17]. Note that the retrieved thermal conductivity was found to be independent of the choice heat flux. The time step was set to 0.55 fs instead of 0.97 fs used in Ref. [17] for comparison purposes and to ensure that the results were converged. Simulations were run at constant number of particles, volume and energy (NVE ensemble) for a total of 4 to 6 million time steps corresponding to a simulation time more than twice as long as in Ref. [17]. The equations of motion were integrated using a velocity Verlet algorithm [4]. The z-direction of the simulation cell was divided into 2 N slices of width equal to the α-quartz lattice parameter in that direction. The temperature of each slice was obtained using Eq. (2) after averaging over the last 2 million steps of the simulation run. Note that the temperature profile was found to have already converged after the first 2 million steps. It was linear except for the slices within 60 Å of the heat source and heat sink regions. The non-linearity in temperature observed around those regions was attributed to the strong scattering caused by the heat source/sink [33]. The linear part of the temperature profile was fitted with a linear function, $T(z)$, and the gradient, dT/dz, was used in Eq. (1) to estimate the thermal conductivity. The gradients estimated for the two different linear regions, on each side of the heat source, typically differed by less than 15%. This difference was used to estimate the error associated with the predicted value of the thermal conductivity. Finally, Eq. (1) was used to estimate the thermal conductivity of α-quartz at 500 and 800 K [34].

Fig. 3 plots the values of $1/k$ as a function of $1/L_z$ predicted at 500 and 800 K and for different simulation cell lengths along with results reported by Yoon et al. [17] and Huang et al. [16]. Error bars
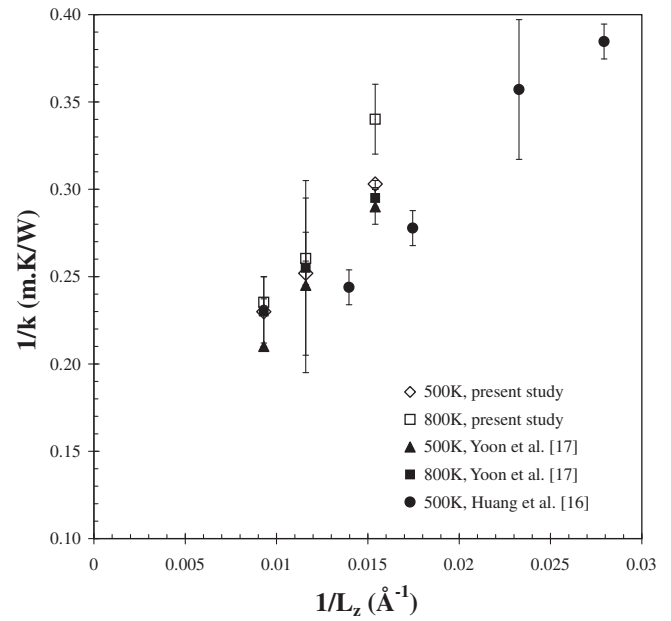
correspond to the error estimates for the thermal conductivity values retrieved from MD simulations. Fig. 3 indicates that all results obtained in the present study but one are within the numerical uncertainty of those previously reported by Yoon et al. [17]. Differences with data reported by Huang et al. [16] are slightly larger. This can be attributed to the fact that the density of the crystalline structure simulated in Ref. [16] was 2,180 kg/m^3 compared with 2,647 kg/m^3 in Ref. [17] and in the present study. In addition, the exact phase and atomic structure were not reported in Ref. [16] and may be different from the α-quartz structure used here and in Ref. [17]. Note that the thermal conductivities computed were relatively small (~3 to 5 W/m · K). Therefore, the differences in $1/k$, observed with Yoon et al.'s data [17] in Fig. 3, actually corresponded to less than 10% relative differences in terms of thermal conductivity.

3.3. Procedure for predicting the thermal conductivity of dense amorphous silica

The first step toward predicting the thermal conductivity of nanoporous amorphous silica consisted of preparing a dense phase of amorphous silica. Then, pores were introduced into the dense phase by removing atoms within selected areas of the simulation cell. The amorphous silica phase was generated following a procedure similar to those described in Refs. [9,14,18,20]. The α-quartz system was heated at a temperature of 10,000 K and subsequently quenched to 300 K. During this process, because of the very large atomic kinetic energy at such high temperatures, atoms may approach each other very closely. The BKS potential, previously used for α-quartz, does not provide large enough repulsive forces at high energies. Therefore, it was modified, for small interatomic distances, to ensure the system's cohesion during melting [9,14]. To do so, a so-called $24 - 6$ Lennard–Jones potential was added to the initial BKS potential given by Eq. (3) to yield [14],

$$V(r_{ij}) = \frac{q_i q_j}{r_{ij}} + A_{ij} exp(-B_{ij} r_{ij}) - \frac{C_{ij}}{r_{ij}^6} + 4\epsilon_{ij} \left[\left(\frac{\sigma_{ij}}{r_{ij}} \right)^{24} - \left(\frac{\sigma_{ij}}{r_{ij}} \right)^6 \right] \quad (4)$$

The parameters ϵ_{ij} and σ_{ij} were the same as those introduced by Guissani et al. [35] and also used by McGaughey et al. [14] and

Mahajan et al. [9]. They were set as ϵ_{SiSi} = 13.20 eV, ϵ_{SiO} = 1.12 × 10^{-2} eV and ϵ_{OO} = 4.78 × 10^{-4} eV; σ_{SiSi} = 0.40 Å, σ_{SiO} = 1.35 Å and σ_{OO} = 2.20 Å [35]. The values of q_i, q_j, A_{ij}, B_{ij} and C_{ij} remained unchanged. It was verified that this modified potential for α-quartz resulted in the same thermal conductivity at 500 and 800 K as that presented in Fig. 3 and obtained without the additional 24 − 6 LJ potential.

Three different approaches were tested to perform the melting and quenching of the initial α-quartz phase using (i) a constant number of particles, pressure, and enthalpy (NPH) ensemble, (ii) a constant number of particles, pressure and temperature (NPT) ensemble, and (iii) a constant number of particles, volume and temperature (NVT) ensemble. Note that the most physically realistic approach consists of performing the melting and quenching processes from the initial α-quartz phase and let the volume expand. However, performing such MD simulations in the NPH or NPT ensemble was found to yield a final density for the amorphous phase ranging between 2,520 and 2,580 kg/m^3. This is significantly larger than the typical density of 2,200 kg/m^3 reported for amorphous silica [36]. This means that the implemented potential was unable to yield spontaneously an amorphous phase with the desired density. Thus, the density was artificially lowered by isotropically expanding the simulation cell in the three Cartesian directions. Moreover, the use of the NPH ensemble was found to make the volume of the simulation cell very unstable at high temperatures and therefore only the NVT and NPT ensembles were used.

When using the NVT ensemble, the density of the initial α-quartz phase was lowered from 2,647 kg/m^3 to 2,200 kg/m^3 [36] before the melting and quenching processes. The last step consisted of letting the system relax, at room temperature, to the zero-pressure condition. This was achieved while performing an energy minimization of the system by iteratively adjusting atoms' coordinates. Since the BKS potential spontaneously gives a density larger than that of amorphous silica at room temperature, the density of the amorphous phase would thus slightly increase during this last minimization step, up to a final value of approximately 2,218 kg/m^3.

On the other hand, when using the NPT ensemble, the melting and quenching were performed from an unmodified initial α-quartz phase. The energy minimization step was subsequently performed. Finally, for comparison purposes, the density of systems obtained using the NPT ensemble was also set to 2,218 kg/m^3 by isotropically expanding the simulation cell, this time, after the melting and quenching processes.

Note that the use of the NVT ensemble was found to be inappropriate to generate amorphous silica systems from strongly anisotropic simulation cells with one dimension being more than five times larger than the two others. Indeed, the BKS potential yielded a spontaneous density of approximately 2,550 kg/m^3. Thus when the system was first expanded to lower its density to 2,200 kg/m^3, it was put under negative pressure. As a consequence, anisotropic systems were found to split in two parts during the quenching process, along the direction of the largest simulation cell dimension. This was avoided in the NPT ensemble where the volume of the simulation cell was allowed to fluctuate at constant pressure.

In both approaches, the system temperature was first set to 10,000 K for 60,000 steps and then progressively lowered to 300 K using a Nose–Hoover thermostat [37,38]. The time step during quenching was set to 0.905 fs by analogy with Ref. [14]. Quenching was performed over three million time steps corresponding to a simulation time of 2.715 ns and a quenching rate of 3.68 × 10^{12} K/s. Note that this quenching rate was lower than that used by Mahajan et al. [9] or Jund and Jullien [18] but remained much larger than that of actual quenching processes. On the other hand, time scales of physical experiments were also shown to be much longer than those of MD simulations [39]. Such a quenching rate was indeed shown in previous studies to generate amorphous silica phases with over 99% of the atoms having the proper coordination [9,14]. Here, it was also verified that simulations performed on amorphous systems generated with four times lower quenching rates predicted identical thermal conductivities.

Similarly, simulations performed on systems melted up to 12,000 K predicted a thermal conductivity at 300 K identical to those obtained after melting at 10,000 K. However, systems melted at 5,000 K, featured thermal conductivities up to seven times larger than those obtained after melting at 10,000 K or more. These observations show that the quenching rate and melting temperature used in this study ensured that the resulting phase was fully amorphous. Fig. 2b shows the atomic structure of a typical dense amorphous silica phase obtained using the above described procedure.

Finally, thermal conductivity of dense silica at 300 K was modeled using the Müller–Plathe method already validated for dense α-quartz. Amorphous silica systems of various sizes were investigated. Each amorphous system was prepared starting from an α-quartz system of the corresponding size. The z-direction of the simulation cell was divided into slices of width ranging from 1.5 to 4.0 Å, depending on the system size. The velocity exchange rate was adjusted to set the heat flux to approximately 3.8 × 10^{11} eV/nm^2 · s (i.e., 6.0 × 10^{10} W/m^2). The time step was set to 0.55 fs and thermal conductivity simulations were run in the NVE ensemble for 4 to 6 million time steps. The procedures used to estimate the temperature gradient and to calculate the thermal conductivity were identical to that previously described α-quartz.

4. Results and discussion

4.1. Thermal conductivity of dense amorphous silica

4.1.1. Thermal conductivity of a cubic system

First, in order to compare our thermal conductivity predictions with those reported by Jund and Jullien [18], an amorphous silica system of 23.4 Å × 22.5 Å × 22.9 Å and n = 648 atoms (216 silicon atoms and 432 oxygen atoms) was simulated. The amorphous system was prepared using the NVT ensemble starting from an α-quartz phase made of 3 × 4 × 4 quartz unit cells in the x-, y- and z-directions, respectively. Our MD simulations predicted a thermal conductivity of 1.20 ± 0.05 W/m · K at room temperature. This was in good agreement with results previously obtained by Jund and Jullien [18] and Huang et al. [16] for systems with similar dimensions and numbers of atoms.

4.1.2. Effect of system length

Fig. 4 shows the thermal conductivity k of amorphous silica systems at 300 K as a function of L_z. The cross-sectional area S of the systems was set to 15.4 × 13.5 Å^2, 23.4 × 22.5 Å^2, or 31.3 × 27.1 Å^2. On the other hand, the length L_z of these systems varied from 17 to 189 Å. For some systems, both the NVT and NPT ensemble methods were used to prepared the amorphous phase. Results previously reported by Huang et al. [16] for systems with cross-section equal to 21.4 × 21.4 Å^2 are also displayed in Fig. 4 for comparison purposes. Error bars correspond to the error estimates for the thermal conductivity values retrieved from MD simulations. Fig. 4 indicates that the thermal conductivity of the dense amorphous silica phase increased as the length of the simulation cell increased. It also establishes that results were independent of the cross-section and of the ensemble used to prepare the amorphous phase. Finally, good agreement was found with results reported by Huang et al. [16]. These simulations show that,
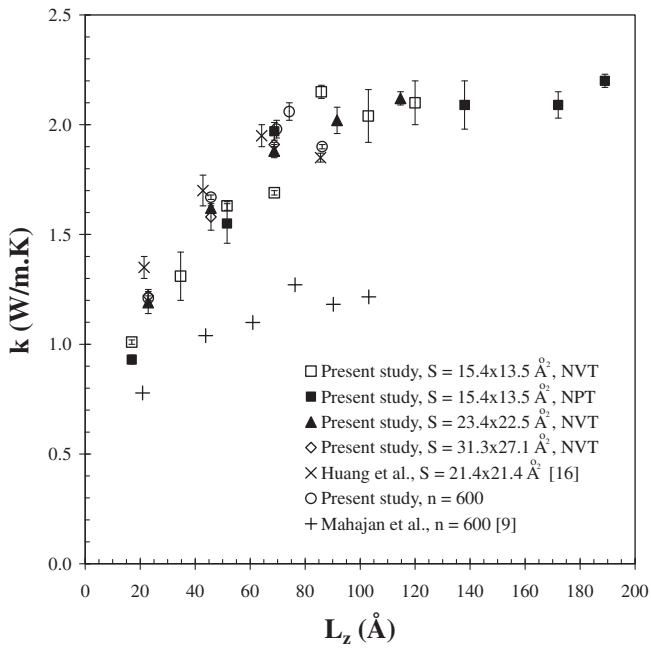
Fig. 4. Predicted thermal conductivity of amorphous silica systems at 300 K as a function of L_z for various cross-sections generated using NVT and NPT ensembles along with results reported in the literature [9,16].

although silica is amorphous, size-effects are still observable for simulation cell lengths smaller than 110 Å. Thermal conductivity reached a plateau for simulation cell lengths larger than 110 Å beyond which it is approximately 2.10 ± 0.10 W/m · K.

Moreover, McGaughey et al. [14] obtained a thermal conductivity of 1.96 W/m · K by applying the Green–Kubo method to an amorphous silica system of 576 atoms. This number of atoms corresponds to the smallest system showed in Fig. 4. As already discussed in Ref. [17], it appears that smaller systems can yield results closer to those of the bulk when using the Green–Kubo method. However, it has also been established that results obtained with the Green–Kubo method are still affected by finite-size effects [11,13,22]. This may explain the slight discrepancy between results reported in Ref. [14] and those obtained in the present study.

Finally, the thermal conductivity predicted by the Green–Kubo method and by non-equilibrium MD simulations overestimate the experimental value of 1.40 W/m · K [40]. As previously suggested by McGaughey et al. [14] and Huang et al. [16], the BKS potential is "somewhat" suitable to simulate amorphous silica.

4.1.3. Thermal conductivity of systems with constant number of atoms

Simulations were also performed for amorphous silica systems of different dimensions but constant number of atoms n similar to those presented by Mahajan et al. [9]. Systems with $n = 600$ atoms approximately, and varying length and cross-section were simulated. The system length L_z varied from 22.9 to 86.0 Å while the cross-section was adjusted to keep the number of atoms nearly constant. MD simulation results as well as data previously reported by Mahajan et al. [9] are displayed in Fig. 4.

Data obtained in the present study confirms that thermal conductivity of the dense amorphous silica phase increases with the length of the simulation cell and that reducing the cross-sectional area of the system did not influence the predictions. However, results where found to disagree with those reported by Mahajan et al. [9] who predicted a maximum thermal conductivity of about 1.20 W/m · K for L_z exceeding 70 Å.

To conclude, this preliminary study showed that results obtained with the method implemented here were in good agreement with those previously reported in the literature [14,16–18]. The modified BKS potential [Eq. (4)] used for dense amorphous silica yielded an amorphous silica phase with (i) a density which was spontaneously larger than actual amorphous silica, and (ii) the predicted bulk thermal conductivity overestimated that experimentally measured at room temperature [40]. However, the BKS potential has been widely used [16,18] and can be used to qualitatively assess the effect of pore diameter and porosity on the thermal conductivity of nanoporous silica.

4.2. Thermal conductivity of amorphous nanoporous silica

In this section, the thermal conductivity of amorphous nanoporous silica systems made of monodisperse spherical pores organized in a simple cubic arrangement was predicted at 300 K for a wide range of system length, pore diameter, and porosity. The pores were simulated as empty, i.e., without any gas molecules inside. This is based on the fact that the thermal conductivity of gas in such confined space, denoted by k_d, is negligibly small as predicted by kinetic theory for very large Knudsen number Kn according to [41],

$$k_d = \frac{k_{d,0}}{1 + 2\beta\mathrm{Kn}} \quad \text{where} \quad \mathrm{Kn} = \frac{\ell}{d_p} = \frac{k_B T}{\sqrt{2}\pi\sigma^2 p d_p} \qquad (5)$$

Here, ℓ is the gas molecule mean free path inside the pores of diameter d_p while p is the pressure, and σ is the diameter of the hard-shell particles representing the gas molecules. The coefficient β is equal to 1.5 for air, and $k_{d,0}$ is the thermal conductivity of bulk air corresponding to Kn = 0.0 and equal to 0.026 W/m · K at atmospheric pressure and room temperature [42]. It is evident that for pores a few nanometer in diameter Kn becomes very large at atmospheric pressure and room temperature resulting in $k_d \approx 0.0$.

4.2.1. Effect of system length and pore diameter

Three different sets of systems corresponding to simulation cells with cross-sectional area S equal to 15.4×13.5 Å^2, 23.4×22.5 Å^2, and 31.4×31.6 Å^2 were studied with length L_z varying from 17 to 189 Å, 22 to 138 Å, and 69 to 138 Å, respectively. The spherical pores' diameter d_p was set to 12 Å, 18 Å, or 25 Å. The pores were all aligned and equally spaced along the centerline of the simulation cell. The heat flux was imposed along the z-direction. Fig. 2c shows the atomic structure of a typical amorphous nanoporous silica phase with two pores 18 Å in diameter in a $23.4 \times 22.5 \times 45.7$ Å^3 simulation cell. The number of pores simulated ranged from 1 to 11. It was adjusted as the length of the simulation cell was increased in order to maintain the porosity f_v at $25 \pm 2\%$. Fig. 5 shows the thermal conductivity k predicted at 300 K as a function of L_z for both dense and nanoporous amorphous silica systems. It establishes that the thermal conductivity of amorphous nanoporous silica systems (i) increased with increasing L_z and (ii) was lower than that of the corresponding dense amorphous systems.

Moreover, Fig. 5 indicates that the thermal conductivity of amorphous nanoporous silica was independent of the pore diameter when the system length was larger than approximately 100 Å. It is particularly interesting to note that the same observations were made experimentally for highly-ordered cubic and hexagonal mesoporous silica thin films with pore diameter and porosity ranging from 3 to 18 nm and from 20% to 48% [3]. It also suggests that a minimum amount of material (or number of atoms and pores) needed to be modeled in order for the amorphous nanoporous medium to behave as homogeneous and continuous with some effective thermal conductivity k_{eff}. Then, effective medium
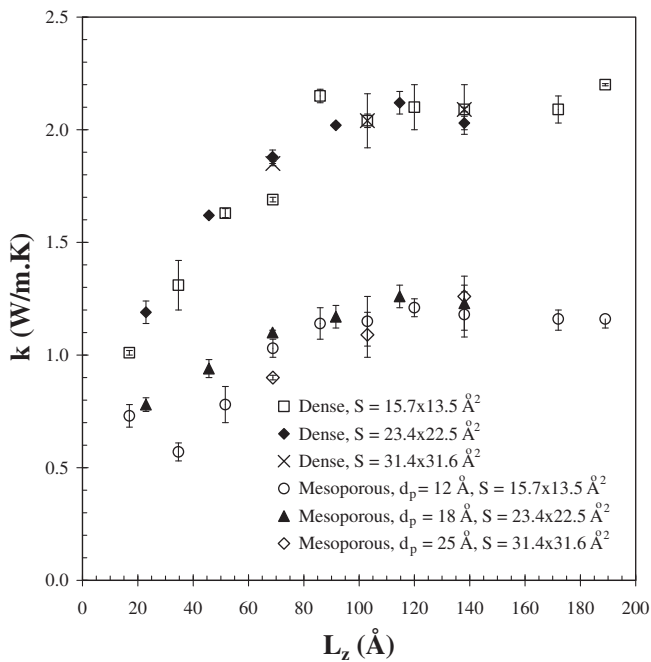
Fig. 5. Predicted thermal conductivity k at 300 K as a function of L_z for amorphous nanoporous silica systems of porosity $f_v = 25 \pm 2\%$ with various values of cross-section S and pore diameter d_p along with that of the corresponding dense amorphous silica systems.

approximation are valid and can be used to model the effect of porosity on thermal conductivity [43,44].

4.2.2. Effect of porosity

Molecular dynamic simulations of amorphous nanoporous silica systems with cross-section $S = 23.4 \times 22.5$ Å² and length $L_z = 114.7$ Å were performed to investigate the influence of porosity on the effective thermal conductivity of amorphous nanoporous silica. For such dimensions, the effective thermal conductivity was previously shown to be independent of the system's length and cross-section as well as of the pore diameter. Therefore, the effect of porosity alone could be investigated. Five pores, all aligned and equally spaced along the centerline of the simulation cell were introduced into the amorphous silica phase. The diameter of the pores varied from 13.3 to 20.1 Å so that the system porosity ranged from 10% to 35%.

Finite element analysis simulations were also performed using COMSOL Multiphysics 3.4. The conventional heat diffusion equation based on continuum theory and Fourier's law was solved in each phase for the same simple cubic arrangements of spherical pores as those modeled with MD simulations (Fig. 2c). Continuous heat flux boundary conditions were imposed at all pore/matrix interfaces. The thermal conductivity of the gas phase k_d was set equal to zero as previously discussed. The thermal conductivity of the matrix k_c was assumed to be 1.4 W/m · K [40].

Results from MD simulations and continuum theory were compared with predictions from various and commonly used EMAs including the parallel model, Maxwell Garnett model [45,41,46], as well as the porosity weighted simple medium (PWSM) model, porosity weighted dilute medium (PWDM) model [47], and the coherent potential approximation [48]. Expressions and physical interpretations of these EMAs were provided in our previous study [3]. Note that the PWDM and PWSM models use a common semi-empirical fitting parameter x which may range from zero to infinity in order to accounts for the cumulative effects of parameters such as pore shape or pore size on thermal conductivity [47]. Also, in

these EMAs, k_d and k_c were taken as 0.0 and 1.4 W/m · K, respectively. Then, the parameter x equals 0.29, was found to provide the best fit of the experimental data. Furthermore, MD simulations predicted the thermal conductivity of dense amorphous silica as $k_c = 2.10$ W/m · K as previously discussed. Therefore, for comparison purposes, both the numerically predicted and experimentally measured effective thermal conductivities k_{eff} of nanoporous silica were scaled by the thermal conductivity of the corresponding dense phase k_c.

Fig. 6 plots the ratio k_{eff}/k_c for amorphous nanoporous silica at 300 K as a function of porosity f_v predicted from (ii) MD simulations, (ii) finite element analysis, (iii) commonly used EMAs, and (iv) previously reported experimental data for amorphous sol–gel mesoporous silica films [3]. In all cases, the thermal conductivity of the amorphous nanoporous silica system decreased with increasing porosity. However, MD simulations, finite element analysis, and experimental measurements give quantitatively different values.

First, Fig. 6 indicates that predictions from finite element analysis agreed well with Maxwell Garnett model given by [45],

$$\frac{k_{eff}}{k_c} = 2\left(\frac{1 - f_v}{2 + f_v}\right) \qquad (6)$$

This was also established analytically by Whitaker [49] using volume averaging theory for porous materials with spherical pores arranged in a cubic lattice. Note that the poor agreement observed between the finite element analysis predictions and experimental data can be explained by the fact that the former was based on Fourier's law and did not account for sub-continuum thermal transport in nanoporous structure.

Moreover, Fig. 6 establishes that the thermal conductivity ratios predicted by MD simulations was in good agreement with the coherent potential approximation [50,43]. For $k_d = 0.0$ W/m · K the latter simplifies to [43],
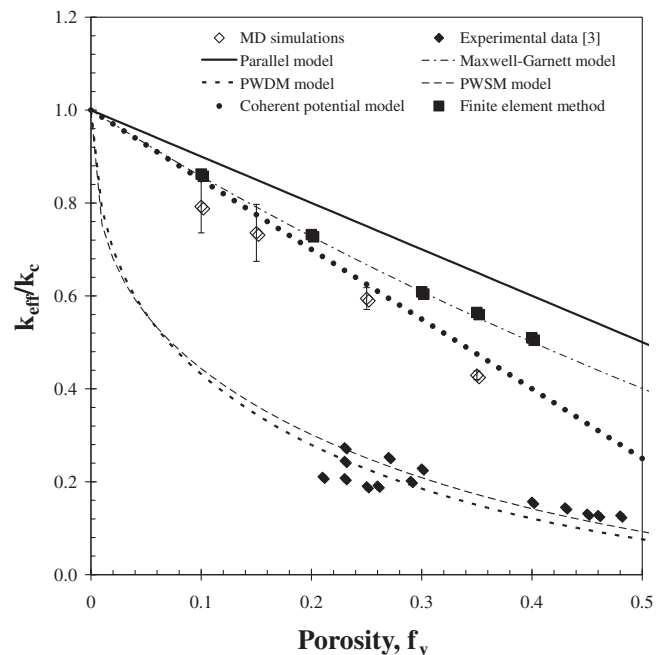

Fig. 6. Predicted thermal conductivity ratio k_{eff}/k_c at 300 K as a function of porosity for amorphous nanoporous silica systems of $23.4 \times 22.5 \times 114.7$ Å³ along with experimental data [3] and predictions from commonly used effective medium approximations.

$$\frac{k_{eff}}{k_c} = 1 - 1.5f_v \tag{7}$$

This EMA was first derived by Landauer [48] and expresses the thermal or electrical conductivity of a composite structure made of a matrix material and spherical inclusions of a second phase. Note that it is also identical to the symmetric Bruggeman model [51] when the thermal conductivity of the dispersed phase k_d is equal to zero. Cahill and Allen [50,43] successfully used Eq. (7) to predict the thermal conductivity of Vycor glass from 30 to 300 K with pore diameter and porosity approximately equal to 10 nm and 30%, respectively.

Furthermore, predictions from MD simulations failed to predict the experimental data. Experimentally, the porous structure of mesoporous silica films is typically a BCC arrangement of quasi-spherical pores connected by narrow necks less than 1 nm in diameter [3]. The necks can be considered as micropores which contribute for a small part to the total porosity but significantly to the surface area per unit volume. They were shown to represent approximately 15% of the total porosity in sol–gel mesoporous silica thin films [52]. However, calculations assuming micropores to be cylindrical with diameters about ten times smaller than the mesopores, show that microporosity accounts for approximately 50% of the total pore surface area. Those necks, which were not modeled in the present simulations, may constitute significant resistance to heat transfer in amorphous sol–gel mesoporous silica and decrease their effective thermal conductivity. Faithfully simulating the actual mesoporous structure would require significantly larger computing resources and time. In addition, simulating the necks presents a major challenge as they may collapse within a few time steps as was observed in the present study for amorphous silica with spherical pores 0.64 nm in diameter.

Finally, note that in actual mesoporous silica films, the surface of the pores is naturally passivated with hydrogen atoms. This was not accounted for in the present MD simulations because of the complexity of the atomic structure of the generated amorphous silica phase. The presence of hydrogen atoms would also require the use of new interaction potentials or increasing the effective mass of Si and/or O atoms located at the pore surface [53]. However, surface passivation is expected to have a very small influence on thermal conductivity at the temperature considered in this study. Indeed, it only concerns a small fraction of the atoms inside the simulation cell and those atoms are located at the surface of the pores whereas heat is mainly transported through the amorphous silica matrix.

5. Conclusion

This paper presented predictions of the effective thermal conductivity of amorphous nanoporous silica at 300 K using non-equilibrium molecular dynamics simulations. Nanoporous silica structures consisting of more than 9,000 atoms and up to 11 pores aligned in the direction of the heat flux were simulated. System length, pore diameter, and porosity varied from 17 to 189 Å, 12 to 25 Å, and 10% to 35%, respectively. The widely used BKS potential was modified with a $24 - 6$ LJ potential to model interatomic interactions in amorphous silica. The thermal conductivity was estimated using the Müller-Plathe method and the procedure was validated against previously reported data for crystalline α-quartz [17] and non-porous amorphous silica [14,16]. The results were independent of the cross-section of the simulation cell and of the ensemble used to generate the amorphous silica phase. The thermal conductivity was also independent of the system length L_z when the latter was larger than 110 Å, for both non-porous and nanoporous silica. The thermal conductivity of nanoporous silica was also found to be independent of pore diameter and

depended only on porosity. It is worth noticing that the same results were observed experimentally for highly-ordered cubic and hexagonal mesoporous silica [3]. Then, nanoporous silica can be treated as a continuous homogeneous medium with some effective thermal conductivity. The thermal conductivity predicted by MD simulations was in good agreement with the coherent potential model given by Eq. (7). On the other hand, predictions by finite element analysis based on continuum theory agreed with the well-known Maxwell Garnett model. Differences between MD simulation predictions and experimental data [3] could possibly be attributed to the presence of "necks" connecting the pores in actual amorphous sol–gel mesoporous silica and ignored in the MD simulations.

References

[1] Semiconductor Industry Association, The international technology roadmap for semiconductors 2006.
[2] S.G. Choi, T.J. Ha, B.G. Yu, S.P. Jaung, O. Kwon, H.H. Park, Improvement of uncooled infrared imaging detector by using mesoporous silica as a thermal isolation layer, Ceramics Int. 34 (4) (2008) 833–836.
[3] T. Coquil, E.K. Richman, N. Hutchinson, S.H. Tolbert, L. Pilon, Thermal conductivity of cubic and hexagonal mesoporous silica thin films, J. Appl. Phys. 106 (3) (2009) 034910.
[4] M.P. Allen, D.J. Tildesley, Computer Simulation of Liquids, Oxford University Press, Oxford, UK, 2002.
[5] M.S. Green, Markoff random processes and the statistical mechanics of time-dependent phenomena. II. Irreversible processes in fluids, J. Chem. Phys. 22 (3) (1954) 398–413.
[6] R. Kubo, M. Yokota, S. Nakajima, Statistical-mechanical theory of irreversible processes. II. Response to thermal disturbance, J. Phys. Soc. Jpn 12 (11) (1957) 1203–1211.
[7] P.K. Schelling, S.R. Phillpot, P. Keblinski, Comparison of atomic-level simulation methods for computing thermal conductivity, Phys. Rev. B 65 (14) (2002) 144306.
[8] F. Müller-Plathe, A simple nonequilibrium molecular dynamics method for calculating the thermal conductivity, J. Chem. Phys. 106 (14) (1997) 6082–6085.
[9] S.S. Mahajan, G. Subbarayan, B.G. Sammakia, Estimating thermal conductivity of amorphous nanoparticles and nanowires using molecular dynamics simulations, Phys. Rev. E 76 (5) (2007) 056701.
[10] R. Vogelsang, C. Hoheisel, G. Ciccotti, Thermal conductivity of the Lennard–Jones liquid by molecular dynamics calculations, J. Chem. Phys. 86 (11) (1987) 6371–6375.
[11] J. Che, T. Çagin, W.A. Goddard III, Thermal conductivity of carbon nanotubes, Nanotechnology 11 (2) (2000) 65–69.
[12] J. Li, L. Porter, S. Yip, Atomistic modeling of finite-temperature properties of crystalline β- SiC: II. Thermal conductivity and effects of point defects, J. Nuclear Mater. 255 (2–3) (1998) 139–152.
[13] S.G. Volz, G. Chen, Molecular-dynamics simulation of thermal conductivity of silicon crystals, Phys. Rev. B 61 (4) (2000) 2651–2656.
[14] A.J.H. McGaughey, M. Kaviany, Thermal conductivity decomposition and analysis using molecular dynamics simulations: Part II. Complex silica structures, Int. J. Heat Mass Transfer 47 (8–9) (2004) 1799–1816.
[15] F.H. Stillinger, T.A. Weber, Computer simulation of local order in condensed phases of silicon, Phys. Rev. B 31 (8) (1985) 5262–5271.
[16] Z. Huang, Z. Tang, J. Yu, S. Bai, Thermal conductivity of amorphous and crystalline thin films by molecular dynamics simulation, Phys. B Condens. Matter 404 (12–13) (2009) 1790–1793.
[17] Y.G. Yoon, R. Car, D.J. Srolovitz, S. Scandolo, Thermal conductivity of crystalline quartz from classical simulations, Phys. Rev. B 70 (1) (2004) 012302.
[18] P. Jund, R. Jullien, Molecular-dynamics calculation of the thermal conductivity of vitreous silica, Phys. Rev. B 59 (21) (1999) 13707–13711.
[19] B.W.H. van Beest, G.J. Kramer, R.A. van Santen, Force fields for silicas and aluminophosphates based on ab initio calculations, Phys. Rev. Lett. 64 (16) (1990) 1955–1958.
[20] W. Horbach, J. Kob, K. Binder, C.A. Angell, Finite size effects in simulations of glass dynamics, Phys. Rev. E 54 (6) (1996) R5897–R5900.
[21] L. Sun, J.Y. Murphy, Domain size effects in molecular dynamics simulation of phonon transport in silicon, Appl. Phys. Lett. 89 (17) (2006) 171919.
[22] D.P. Sellan, E.S. Landry, J.E. Turney, A.J.H. McGaughey, C.H. Amon, Size effects in molecular dynamics thermal conductivity predictions, Phys. Rev. B 81 (21) (2010) 214305.
[23] J.R. Lukes, C.L. Tien, Molecular dynamics simulation of thermal conduction in nanoporous thin films, Microsc. Thermophys. Eng. 8 (4) (2004) 341–359.

[24] J.H. Lee, J.C. Grossman, J. Reed, G. Galli, Lattice thermal conductivity of nanoporous Si: molecular dynamics study, Appl. Phys. Lett. 91 (22) (2007) 223110.

[25] J.A. Thomas, J.E. Turney, R.M. Iutzu, C.H. Amon, A.J.H. McGaughey, Predicting phonon dispersion relations and lifetimes from the spectral energy density, Phys. Rev. B 81 (8) (2010) 081411.

[26] J.A. Thomas, R.M. Iutzu, A.J.H. McGaughey, Thermal conductivity and phonon transport in empty and water-filled carbon nanotubes, Phys. Rev. B 81 (4) (2010) 045413.

[27] J.R. Lukes, H. Zhong, Thermal conductivity of individual single-wall carbon nanotubes, ASME J. Heat Transfer 129 (2007) 705–716.

[28] Y. He, D. Donadio, G. Galli, Heat transport in amorphous silicon: interplay between morphology and disorder, Appl. Phys. Lett. 98 (14) (2011) 144101.

[29] J.R. Lukes, D.Y. Li, X.-G. Liang, C.-L. Tien, Molecular dynamics study of solid thin-film thermal conductivity, ASME J. Heat Transfer 122 (3) (2000) 536–543.

[30] S.J. Plimpton, Fast parallel algorithms for short-range molecular dynamics, J. Comput. Phys. 117 (1995) 1–19. http://lammps.sandia.gov.

[31] R.W. Hockney, J.W. Eastwood, Computer Simulation Using Particles, Adam Hilger, New York, NY, 1989.

[32] L. Levien, C.T. Prewitt, D.J. Weidner, Structure and elastic properties of quartz at pressure, P = 1 atm, Am. Mineral. 64 (1980) 920–930.

[33] C. Oligschleger, J.C. Schön, Simulation of thermal conductivity and heat transport in solids, Phys. Rev. B 59 (6) (1999) 4125–4133.

[34] M.H. Müser, Simulation of material properties below the debye temperature: a path-integral molecular dynamics case study of quartz, J. Chem. Phys. 114 (14) (2001) 705–716.

[35] Y. Guissani, B. Guillot, A numerical investigation of the liquid–vapor coexistence curve of silica, J. Chem. Phys. 104 (19) (1996) 7633–7644.

[36] J.F. Shackelford, W. Alexander (Eds.), CRC Materials Science and Engineering Handbook, 3rd ed., CRC Press, Boca Raton, FL, 2000.

[37] S. Nose, A unified formulation of the constant temperature molecular dynamics methods, J. Chem. Phys. 81 (1) (1984) 511–519.

[38] W.G. Hoover, Canonical dynamics: equilibrium phase-space distributions, Phys. Rev. A 31 (1985) 1695–1697.

[39] K. Vollmayr, W. Kob, K. Binder, Cooling-rate effects in amorphous silica: a computer-simulation study, Phys. Rev. B 54 (22) (1996) 15808–15827.

[40] Y.S. Touloukian, R.W. Powell, C.Y. Ho, P.G. Klemens, Thermal Conductivity: Nonmetallic Solids, TPRC Data Series, Vol. 2, Plenum, New York, NY, 1970.

[41] B. Nait-Ali, K. Haberko, H. Vesteghem, J. Absi, D.S. Smith, Thermal conductivity of highly porous zirconia, J. Eur. Ceramic Soc. 26 (16) (2006) 3567–3574.

[42] M. Kaviany, Principles of Heat Transfer, John Wiley & Sons, New York, NY, 2002.

[43] D.G. Cahill, Heat transport in dielectric thin films and at solid-solid interfaces, in: C.L. Tien, A. Majumdar, F.M. Gerner (Eds.), Microscale Energy Transport, Taylor and Francis, Washington, DC, 1998, pp. 85–118.

[44] R.M. Costescu, A.J. Bullen, G. Matamis, K.E. O'Hara, D.G. Cahill, Thermal conductivity and sound velocities of hydrogen-silsesquioxane low-k dielectrics, Phys. Rev. B 65 (9) (2002) 094205.

[45] J.C. Maxwell Garnett, Colours in metal glasses and in metallic films, Phil. Trans. Roy. Soc. Lond. A 203 (1904) 385–420.

[46] C.W. Nan, R. Birringer, D.R. Clarke, H. Gleiter, Effective thermal conductivity of particulate composites with interfacial thermal resistance, J. Appl. Phys. 81 (10) (1997) 6692.

[47] C. Hu, M. Morgen, P.S. Ho, A. Jain, W.N. Gill, J.L. Plawsky, P.C. Wayner, Thermal conductivity study of porous low-k dielectric materials, Appl. Phys. Lett. 77 (2000) 145–147.

[48] R. Landauer, The electrical resistance of binary metallic mixtures, J. Appl. Phys. 23 (7) (1952) 779–784.

[49] S. Whitaker, The Method of Volume Averaging, in: J. Bear (Ed.), Theory and Applications of Transport in Porous Media, vol. 13, Kluwer Academic Publisher, Dordrecht, The Netherlands, 1999.

[50] D.G. Cahill, T.H. Allen, Thermal conductivity of sputtered and evaporated SiO_2 and TiO_2 optical coatings, Appl. Phys. Lett. 65 (3) (1994) 309–311.

[51] D.A.G. Bruggeman, Berechnung verschiedener physikalischer konstanten von heterogenen substanzen. I. D ielektrizitStskonstanten und leitfähigkeiten der mischkörper aus isotropen substanzen, Annalen der Physik (Leipzig) 416 (7) (1935) 636–664.

[52] B. Smarsly, C. Goltner, M. Antonietti, W. Ruland, E. Hoinkis, SANS investigation of nitrogen sorption in porous silica, J. Phys. Chem. B 105 (4) (2001) 831–840.

[53] W.J. Evans, L. Hu, P. Keblinski, Thermal conductivity of graphene ribbons from equilibrium molecular dynamics: effect of ribbon width, edge roughness, and hydrogen termination, Appl. Phys. Lett. 96 (20) (2010) 203112.